Dalton Transactions

PAPER

View Article Online
View Journal | View Issue

Cite this: *Dalton Trans.*, 2017, **46**, 8524

Copper ion interaction with the RNase catalytic site fragment of the angiogenin protein: an experimental and theoretical investigation†

Antonio Magrì,[a] Giovanni Tabbì,[a] Raffaella Breglia,[b] Luca De Gioia,[c] Piercarlo Fantucci,[c] Maurizio Bruschi,*[b] Raffaele P. Bonomo*[d] and Diego La Mendola *[e]

The angiogenin protein (Ang) is a member of the vertebrate-specific secreted ribonucleases and one of the most potent angiogenic factors known. Ang is a normal constituent of human plasma and its concentration increases under some physiological and pathological conditions to promote neovascularization. Ang was originally identified as an angiogenic tumour factor, but its biological activity has been found to extend from inducing angiogenesis to promoting cell survival in different neurodegenerative diseases. Ang exhibits weak ribonucleolytic activity, which is critical for its biological functions. The RNase catalytic sites are two histidine residues, His-13 and His-114, and the lysine Lys-40. Copper is also an essential cofactor in angiogenesis and influences angiogenin's biological properties. The main Cu(II) anchoring site of Ang is His-114, where metal binding inhibits RNase activity of the protein. To reveal the Cu(II) coordination environment in the C-terminal domain of the Ang protein, we report on the characterization, by means of potentiometric, voltammetric, and spectroscopic (CD, UV-Vis and EPR) methods and DFT calculations, of Cu(II) complexes formed with a peptide fragment including the Ang sequence 112–117 (PVHLDQ). Potentiometric titrations indicated that [CuLH$_{-2}$] is the predominant species at physiological pH. EPR, voltammetric data and DFT calculations are consistent with a CuN_3O_2 coordination mode in which a distorted square pyramidal arrangement of the peptide was observed with the equatorial positions occupied by the nitrogen atoms of the deprotonated amides of the Asp and Leu residues, the δ-N atom of histidine and the oxygen atom of the aspartic carboxylic group. Moreover, two analogous peptides encompassing the PVHLNQ and LVHLDQ sequences were also characterized by using thermodynamic, spectroscopic and DFT studies to reveal the role they play in Cu(II) complex formation by the carboxylate side chain of the Asp and Pro residues, a known breaking-point in metal coordination.

Received 4th April 2017,
Accepted 4th June 2017

DOI: 10.1039/c7dt01209h

rsc.li/dalton

Introduction

Angiogenin (Ang) is a multifunctional protein member of the ribonuclease family and shares 33% sequence identity and around 65% homology with pancreatic RNase.[1,2] It is a single-chain protein containing 123 amino acids normally present in human plasma (a concentration of 250–360 μg L^{-1}).[3] Ang is one of the most potent angiogenic factors *in vivo* and it is also required for cell proliferation induced by other angiogenic agents such as vascular endothelial growth factor (VEGF) and basic fibroblast growth factor (bFGF).[4]

Ang plays an important role in tumor angiogenesis[3,5,6] and its expression is up-regulated in many types of cancers; as a matter of fact, the protein was first isolated from a colon adenocarcinoma cell line.[7] Angiogenesis is a complex multistep process in which new blood capillaries grow from pre-existing vessels[8] and the precise molecular pathways by which human angiogenin (hAng) affects these processes are not yet fully understood.[3] Three distinct regions of the protein seem to be necessary to exercise angiogenic activity: the catalytic site for RNase activity involving residues His-13, Lys-40 and His-114, the putative cell binding region encompassing residues

[a]*Consiglio Nazionale delle Ricerche, Istituto di Biostrutture e Bioimmagini (IBB-CNR), Via P. Gaifami 18, 95126 Catania, Italy*
[b]*Dipartimento di Scienze dell'Ambiente e della Terra, Università di Milano-Bicocca, Piazza della Scienza 1, 20126 Milan, Italy. E-mail: maurizio.bruschi@unimib.it*
[c]*Dipartimento di Biotecnologie e Bioscienze, Università di Milano-Bicocca, Piazza della Scienza 2, 20126-Milan, Italy*
[d]*Dipartimento di Scienze Chimiche, Università degli Studi di Catania, Viale A. Doria 6, 95125 Catania, Italy. E-mail: rbonomo@unict.it*
[e]*Dipartimento di Farmacia, Università di Pisa, Via Bonanno Pisano 6, 56126 Pisa, Italy. E-mail: lamendola@farm.unipi.it*

†Electronic supplementary information (ESI) available. See DOI: 10.1039/c7dt01209h

60–68 (KNGNPHREN) and the nuclear translocation sequence 31–35 (RRRGL).[2,9] However, the functional role of Ang is not limited to inducing angiogenesis,[10,11] considering that it plays an essential role in neurite growth[12] and it has a protective role in the brain and spinal cord.[13] Indeed, Ang is down-regulated both in Parkinson's[14] mouse model and in patients affected by Alzheimer's disease (AD).[15] Recently, it has been reported that higher plasmatic Ang levels are associated with AD risk.[16]

Furthermore, Ang mutations have been identified in amyotrophic lateral sclerosis (ALS) patients, and the protein may act as a protective factor for motoneurons.[17–19] It is known that copper homeostasis is involved in neurodegenerative diseases and the metal is also an essential angiogenesis cofactor *in vivo*.[20,21] Serum copper levels are increased in a wide variety of human cancers, and metal chelating agents have been tested as potential anti-cancer drugs, acting through angiogenesis inhibition.[22,23] Interestingly, copper is the only metal in the cytosol moved towards extracellular space during angiogenesis;[24] therefore, metal binding to a protein circulating in the plasma and involved in angiogenesis, such as Ang, may be a pathway the metal takes in angiogenic signalling processes. It has been reported that the Ang protein binds tightly to about 2.4 copper ions per molecule at physiological pH, and protein Cu(II) binding largely increases its interaction with endothelial cells and so its angiogenic activity.[25,26]

We have characterized copper(II) complexes with peptide fragments owing to the Ang putative binding site (residues 60–68, sequence KNGNPHREN)[27,28] and the first α-helix region of protein,[29,30] showing that they are able to tightly bind copper ions. However, it has also been hypothesized that copper and hAng would act along different biological pathways without direct interaction between them in promoting angiogenic processes.[31]

It has to be noted that most data on angiogenic activity reported to date have been obtained using the recombinant form of protein (r-Ang) which contains an extra methionine as the first residue which is not present in plasma Ang.[32]

The effective wild-type protein (wt-Ang) starts with a glutamine residue which spontaneously cyclizes to pyroglutamate, so that wt-Ang has no free amino terminal group.[32]

Different spectroscopic techniques showed that the two proteins bind copper with a different coordination mode: (i) r-Ang binds Cu(II) through the terminal amino group of the extra methionine residue; (ii) the wild-type protein binds Cu(II) through His-114.[33] This residue is one of the three constituents of the RNase catalytic site essential to the protein for carrying out its angiogenic activity and the addition of copper decreases protein RNase activity and capillary-like tube formation.[33] Furthermore, the Cu(II) ion increases the expression of wt-Ang and modulates its intracellular localization in HUVEC, suggesting that metal binding might favour protein internalization,[34] which is a necessary step for Ang to perform its angiogenic activity.[35]

The protein may be internalized as a copper complex when the metal is reduced to Cu(I) in a redox-cycling process closely related to the metal coordination environment and geometry.[36,37]

It has to be noted that in the copper binding with wt-Ang are also involved one/two deprotonated nitrogen atoms, owing to the main anchoring site, His-114, while His-13 and/or His-8 may complete the Cu(II) tetragonal coordination mode.[33]

Therefore, to elucidate the coordination environment of the main Cu(II) binding site within the wt-Ang normally present in human plasma, namely the His-114 as determined by NMR measurements, we synthesised the peptide fragment Ac-PVHLDQ-NH_2 encompassing sequence 112–117 of the protein's C-terminal domain, and its copper(II) complex species was characterized by means of a combined potentiometric, spectroscopic (EPR, CD, UV-Vis), voltammetric and theoretical DFT study.

Cu(II) peptide complexes might form different isomers as amide nitrogen deprotonation can occur towards the N- or the C-terminus. With both a carboxylic side chain and a proline at the N-terminus, deprotonation towards the C-terminus may be favoured. Indeed, the proline residue, containing a secondary nitrogen, acts as a breaking point in the copper coordination within a peptide chain, rendering the formation of a metal–amide nitrogen bond impossible.[38,39]

The formation of different Cu(II) chelate species may favour the distortion of copper(II) tetragonal geometry and/or stabilize square pyramidal geometry, determining different redox properties of the metal which may tune biological processes as determined for prion proteins.[40]

Prompted by the above considerations, the peptide fragments Ac-PVHLNQ-NH_2 in which the aspartic residue (D) was substituted by an asparagine residue (N) and Ac-LVHLDQ-NH_2, where the proline residue (P) was substituted by a leucine (L), were also synthesized and characterized to highlight the role of the aspartic carboxylic side chain and amide nitrogen atoms in copper binding. It is worth noting that P112L single point mutation of this last sequence has been observed in patients affected by ALS.[19]

Experimental

Materials

All *N*-fluorenylmethoxycarbonyl (Fmoc)-protected amino acids, and 2-(1-*H*-benzotriazole-1-yl)-1,1,3,3-tetramethyluronium tetrafluoroborates (TBTU), were obtained from Novabiochem (Switzerland); Fmoc-PAL-PEG resin, *N*,*N*-diisopropylethylamine (DIEA), *N*,*N*-dimethylformamide (DMF, peptide synthesis grade) and a 20% piperidine–DMF solution were from Applied Biosystems; *N*-hydroxybenzotriazole (HOBT), triisopropylsilane (TIS), and trifluoroacetic acid (TFA) were purchased from Sigma-Aldrich. All other chemicals were of the highest available grade and were used without further purification.

Peptide synthesis and purification

The Ac-PVHLDQ-NH_2, Ac-PVHL**N**Q-NH_2 and Ac-**L**VHLDQ-NH_2 peptides were synthesized in *N*-acetylated and *C*-amidated

forms to avoid end-group effects and to more closely mimic their character of an internal protein fragment. They were assembled by the solid phase peptide synthesis strategy using a Pioneer™ Peptide Synthesiser. All amino acid residues were added according to the TBTU/HOBT/DIEA activation method for Fmoc chemistry on Fmoc-PAL-PEG resin (loading 0.22 mmol g^{-1}, 0.33 mmol scale synthesis, 1.5 g of resin). Other experimental details have been reported elsewhere.[41] The peptides were purified by means of preparative reversed-phase high-performance liquid chromatography (rp-HPLC). Purification was done using a Varian PrepStar 200 model SD-1 chromatography system equipped with a Prostar photodiode array detector detecting at 222 nm. The peptide was eluted with solvent A (0.1% TFA in water) and B (0.1% TFA in acetonitrile) on a Vydac C_{18} 250 × 22 mm (300 Å pore size, 10–15 μm particle size) column at a flow rate of 10 mL min^{-1}. Analytical rp-HPLC analyses were performed using a Waters 1525 instrument equipped with a Waters 2996 photodiode array detector detecting at 222 nm. The peptide samples were analysed using gradient elution with solvents A and B on a Vydac C_{18} 250 × 4.6 mm (300 Å pore size, 5 μm particle size) column at a flow rate of 1 mL min^{-1}. The peptides were eluted according to the following protocol: from 0 to 5 minutes isocratic gradient in 0% B, then linear gradient from 0 to 15% B over 15 min, and finally, isocratic gradient in 15% B from 20 to 30 minutes. The peptides (Chart 1) were characterized by using Electron Spray Ionization Mass Spectrometry (ESI-MS).

Ac-PVHLDQ-NH_2: [R_t = 22.03 min]. Calculated mass for $C_{33}H_{52}N_{10}O_{10}$ M = 748.8, ESI-MS [obsd m/z: $(M + H)^+$ 749.7].

Ac-PVHL**N**Q-NH_2: [R_t = 25.14]. Calculated mass for $C_{33}H_{53}N_{11}O_9$ M = 747.8, ESI-MS [obsd m/z: $(M + H)^+$ 748.8].

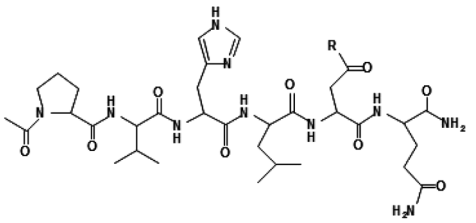

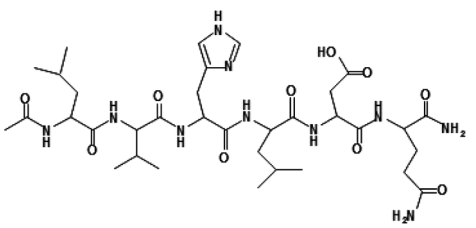

Chart 1 Schematic view of the primary sequence of the investigated peptides.

Ac-**L**VHLDQ-NH_2: [R_t = 23.25]. Calculated mass for $C_{34}H_{57}N_{11}O_9$ M = 763.9, ESI-MS [obsd m/z: $(M + H)^+$ 764.8].

Potentiometric titrations

Potentiometric titrations were performed with home-assembled fully automated apparatus (a Metrohm E654 pH-meter, a combined micro pH glass electrode, Orion 9103SC, and a Hamilton digital dispenser, Model 665) controlled by an appropriate software setup in our laboratory. The titration cell (2.5 ml) was thermostated at 298.0 ± 0.2 K, and all solutions were kept under an atmosphere of argon, which was bubbled through a solution of the same ionic strength and temperature as the measuring cell. KOH solutions (0.1 M) were added through a Hamilton burette equipped with a 1 cm^3 syringe. The ionic strength of all solutions was adjusted to 0.10 M (KNO_3). To determine the stability constants, solutions of the ligands (protonation constants) or the ligands with Cu(II) (copper complex constants) were titrated with 0.1 M potassium hydroxide. The ligand concentration ranged from 1 to 1.5 × 10^{-3} and from 1.5 to 2 × 10^{-3} M for the protonation and complexation experiments. A minimum of three independent runs were performed to determine the protonation constants, while four independent experiments were run for the Cu(II) complexation constants. Metal to ligand ratios ranging between 1 : 1 and 1 : 1.2 were employed. The initial pH was always adjusted to 2.4. To avoid systematic errors and verify reproducibility, the EMF values of each experiment were taken at different time intervals. To obtain protonation and complexation constants, the potentiometric data were refined using HYPERQUAD[42] which minimizes the error square sum of the measured electrode potentials through a non-linear iterative refinement of the sum of the squared residuals, U, and also allows for the simultaneous refinement of data from different titrations:

$$U = \sum (E_{exp} - E_{calc})^2$$

where E_{exp} and E_{calc} are the experimental and calculated electrode potentials. Errors in stability constant values are reported as three times the standard deviations. The formation reaction equilibria of ligands with protons and Cu(II) ions are given in eqn (1):

$$pCu + qH + rL \rightleftarrows Cu_pH_qL_r \quad (1)$$

in which L is the peptides. The stability constant β_{pqr} is defined in eqn (2):

$$\beta_{pqr} = [Cu_pH_qL_r]/[Cu]^p \cdot [H]^q \cdot [L]^r. \quad (2)$$

Species distribution as a function of pH was obtained by using the Hyss program.[43]

Spectroscopic studies

UV-Vis spectra were recorded at 25 °C by using an Agilent 8453 or a Varian Cary 500 spectrophotometer. The peptide and Cu(II) concentrations to record the absorption spectra were the same as those in the potentiometric titrations. Combined spec-

troscopic and potentiometric metal-complex titrations were performed in a 3 ml quartz cuvette with 1 cm path length to obtain a visible region spectrum at each pH value simultaneously. These experiments were replicated at least three times for each copper-peptide. The spectroscopic data were processed by the HYPERQUAD program.[42]

CD spectra were obtained at 25 °C in a constant nitrogen flow on a Jasco model 810 spectropolarimeter at a scan rate of 50 nm min^{-1} and a resolution of 0.1 nm, the path length being 1 cm, in the 280–800 nm range. The spectra were recorded as the average of either 3 or 5 scans. The instrument was calibrated with a 0.06% aqueous solution of ammonium camphorsulfonate. The CD spectra of the Cu(II) complexes were obtained in the 260–800 nm wavelength region as the pH was varied. All the solutions were freshly prepared using double distilled water. Cu(II) and peptide concentrations for the CD spectra in the visible region were identical to those used in the potentiometric titrations. The results are reported as ε (molar absorption coefficient) and $\Delta\varepsilon$ (molar dichroic coefficient) in M^{-1} cm^{-1}.

EPR measurements were carried out by using a Bruker Elexsys E500 CW-EPR spectrometer driven by a PC running the XEpr program under Linux and equipped with a Super-X microwave bridge, operating at 9.3–9.5 GHz, and a SHQE cavity. All the EPR spectra of frozen solutions of Cu(II) complexes were recorded at 150 K by means of an ER4131VT variable temperature apparatus. EPR magnetic parameters were obtained directly from the experimental EPR spectra, calculating them from the 2nd and 3rd lines to avoid second order effects. The instrument settings for the EPR spectra recordings of the copper(II)–peptide complexes were as follows: the number of scans 1–5; microwave frequency 9.344–9.376 GHz; modulation frequency 100 kHz; modulation amplitude 0.2–0.6 mT; time constant 164–327 ms; sweep time 2.8 min; microwave power 20–40 mW; receiver gain 50–60 dB. Copper(II)–peptide complexes were prepared by adding an appropriate amount of isotopically pure copper, taken from a 0.05 M $^{63}Cu(NO_3)_2$ solution, to the peptide solution. The copper(II)–peptide complex solutions were prepared at 1 : 1 metal-to-ligand ratio in the concentration range 0.5–2 mM. The aqueous solution's pH was adjusted by adding NaOH for maximizing the formation percentage of the Cu(II) species. Up to 10% methanol was added to these aqueous solutions to enhance spectral resolution at low temperatures.

Cyclic voltammograms (CV) of the copper(II)–peptide complexes in solution (0.1 M KNO_3 as the ground electrolyte) were recorded by using a BAS CV-50 W voltammetric analyser equipped with a C3 cell stand driven by a standard PC. Copper(II)–peptide complex solutions (0.5×10^{-3} M) were analysed by using a 2 ml BAS glass cell with a three electrode assembly: a glassy carbon working electrode (1 mm diameter), a platinum auxiliary electrode and a standard Ag/AgCl reference electrode. Complex solutions were degassed by using ultra-pure nitrogen bubbled through a three bubbler set filled with a supporting electrolyte solution. CV with a sweep rate of 0.020 V s^{-1} were recorded in the region from +0.5 to −0.9 V. All experiments were carried out at 25 °C. The square wave voltammetry experiments were run in the same potential range as the CV experiments, by using 15 Hz frequency and 25 mV applied pulse values. All potentials in the paper are referenced to the Ag/AgCl reference electrode, +0.215 V *vs*. Normal Hydrogen Electrode (NHE), unless otherwise stated. All Cu(II) complexes, with the exception of the copper hexa-aqua ion, underwent one-electron reduction as derived from the square wave voltammetry (SWV) experiments with the peak width at half-height in the range 102–130 mV. Moreover, these reductions are quasi-reversible because in our CV, the peak-to-peak difference was certainly larger than 60 mV but did not exceed 220 mV, even if anode to cathode peak ratios were often lower than unity, ranging from 0.3 to 0.9. This means that reducing to the lower oxidation state may be complicated by ligands disassociating from the copper(I) species, even if the Cu(II) complex was entirely reclaimed at the end of the oxidation process.

DFT calculations

Calculations were made for the $[Cu(Ac\text{-}PVHLDQ\text{-}NH_2)H_{-2}]^-$, $[Cu(Ac\text{-}PVHL\mathbf{N}Q\text{-}NH_2)H_{-2}]^0$, and $[Cu(Ac\text{-}\mathbf{L}VHLDQ\text{-}NH_2)H_{-2}]^-$ complexes, considering different conformations and coordination modes as explained in the Results and discussion section. The protocol adopted for optimization of the structures consisted of four steps: (i) the structures of the complexes were optimized *in vacuo* according to Density Functional Theory (DFT) using the BP86[44,45] functional in conjunction with the resolution-of-the-identity (RI) technique[46] and the SVP basis set;[47] (ii) 22 water molecules were randomly distributed around the complex within a sphere of 11 Å and their spatial location was optimized *via* a Simulated Annealing (SA) run using the total energy computed according to the DFTB Hamiltonian,[48–53] in which parameters for the atom pairs formed by H, C, N, and O were those of the mio-0-1 set available at http://www.dftb.org[48,51] and those for the pairs Cu–X (X = Cu, H, C, N, O) were those previously reported;[54] (iii) the disposition of the 22 water molecules was optimized at the DFTB level (in (ii) and (iii) the structures of the complexes were frozen in their best DFT *in vacuo* geometries); (iv) and the structures of entire systems (complexes and water molecules) were relaxed at the DFT level (BP86/SVP). EPR parameters were calculated on the DFT geometries optimized both *in vacuo* and with the 22 water molecules using the B3LYP hybrid functional.[55–58]

An extended basis set (14s, 10p, 5d),[47] augmented by a set of diffuse s, p and d functions (with exponents equal to 0.01, 0.03087, and 0.1, respectively) and contracted to (9s, 7p, 4d), was adopted for the Cu atom. The IGLO-II basis was adopted for all other atoms.[59] This basis set will be referred to as BS1 throughout the text. EPR hyperfine coupling constants (hcc) were calculated taking Spin–Orbit (SO) contributions into account, using the one-centre and mean field approximation (AMFI)[60] for the two electron terms (see ref. 61 for a complete discussion of the SO operators). For the calculations of *g* tensors, the gauge origin was set to the centre of electronic charge. DFT geometry optimizations and energy calculations

were performed using the TURBOMOLE 6.4 [62] program suite; DFTB calculations were performed with the DFTB+ program;[52] EPR parameters were calculated using the ORCA program.[63]

Results and discussion

Protonation and Cu(II) equilibria

The protonation constants of the three peptides were determined by potentiometric titrations and are reported in Table 1.

As expected in the investigated pH range, Ac-PVHLDQ-NH_2 and Ac-**L**VHLDQ-NH_2 have two protonation sites, the histidine imidazole nitrogen and aspartic carboxylate moieties, whereas Ac-PVHL**N**Q-NH_2 has only the histidine imidazole nitrogen. The carboxylate and the imidazole groups of Ac-PVHLDQ-NH_2 and Ac-**L**VHLDQ-NH_2 show pK values similar to those reported in the literature.[64,65] The imidazole pK value in Ac-PVHL**N**Q-NH_2 is lower in comparison with that reported for Ac-PVHLDQ-NH_2, and in agreement with the overall different charge of the peptide.[66]

All the peptide fragments have N- and C-termini blocked by acetylation and amidation, so the main anchoring group for copper ion coordination is always the histidine imidazole residue. It is worth noting that under the same experimental conditions, both peptides encompassing the aspartate residue, Ac-PVHLDQ-NH_2 and Ac-**L**VHLDQ-NH_2, start to coordinate at pH values (around pH 4) lower than Ac-PVHL**N**Q-NH_2, which lacks the aspartic (D) residue bearing the carboxylate moiety (Fig. 1).

The first complex species for Ac-PVHLDQ-NH_2 and Ac-**L**VHLDQ-NH_2 has a stoichiometry of $[CuL]^+$, corresponding to the deprotonation of the histidine imidazole nitrogen and the carboxylate group of the aspartate residue. Interestingly, this

Table 1 log pK (n m^{-1}) β and pK values for protonation and complexation with Cu(II) of Ac-PVHLDQ-NH_2, Ac-PVHL**N**Q-NH_2 and Ac-LVHLDQ-NH_2 at 298 K and I = 0.1 M (KNO_3)[a]

Species	Ac-PVHLDQ-NH_2 log β	Ac-PVHL**N**Q-NH_2 log β	Ac-**L**VHLDQ-NH_2 log β
LH	6.64 (1)	6.43 (1)	6.56 (1)
LH_2	10.42 (2)	—	10.27 (1)
pK_{His}	6.64	6.43	6.56
pK_{COO^-}	3.78	—	3.71
[CuL]	4.30 (3)	3.08 (6)	4.53 (1)
$[CuLH_{-1}]$	—	−2.96 (3)	−2.72 (3)
$[CuLH_{-2}]$	−9.14 (3)	−9.09 (2)	−9.08 (3)
$[CuLH_{-3}]$	−19.25 (3)	−19.50 (3)	−18.92 (3)
Step	**pK (n m^{-1})**	**pK (n m^{-1})**	**pK (n m^{-1})**
$pK_{0/-1}$	—	6.04	7.25
$pK_{-1/-2}$	—	6.13	6.37
$pK_{-2/-3}$	10.11	10.41	9.84

values reflect the pK values of Cu(II) complexes. [a] Standard deviations (3σ values) are given in parentheses. Charges are omitted for clarity.

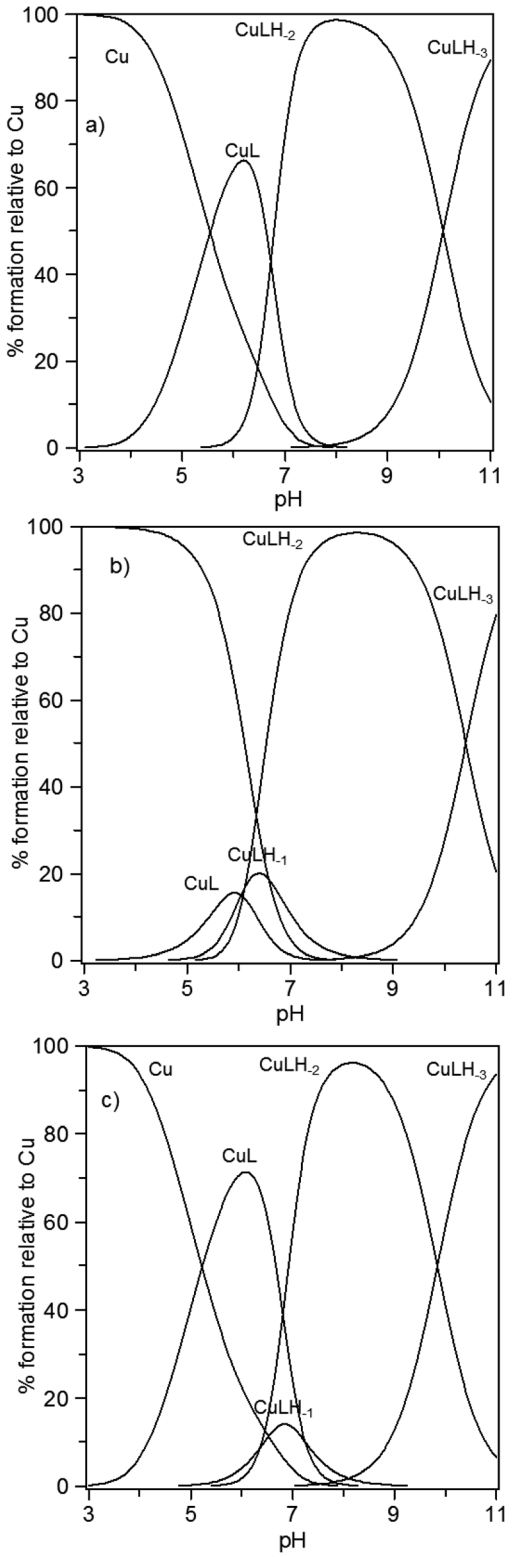

Fig. 1 Species distribution diagrams for Cu(II) complexes ([L] = [M] = 1 × 10^{-3} M) with (a) Ac-PVHLDQ-NH_2, (b) Ac-PVHL**N**Q-NH_2 and (c) Ac-LVHLDQ-NH_2.

copper complex species proves to be the prevailing species up to pH 6.5. The equilibrium reaction $Cu^{2+} + L \rightleftarrows CuL^{2+}$ for Ac-PVHLDQ-NH_2 and Ac-**L**VHLDQ-NH_2 has $\log\beta$ = 4.30 and 4.53, respectively. These values are higher than those generally reported for coordinating only one imidazole nitrogen atom, thus suggesting that there are other donor atoms besides water oxygen atoms.[67–69]

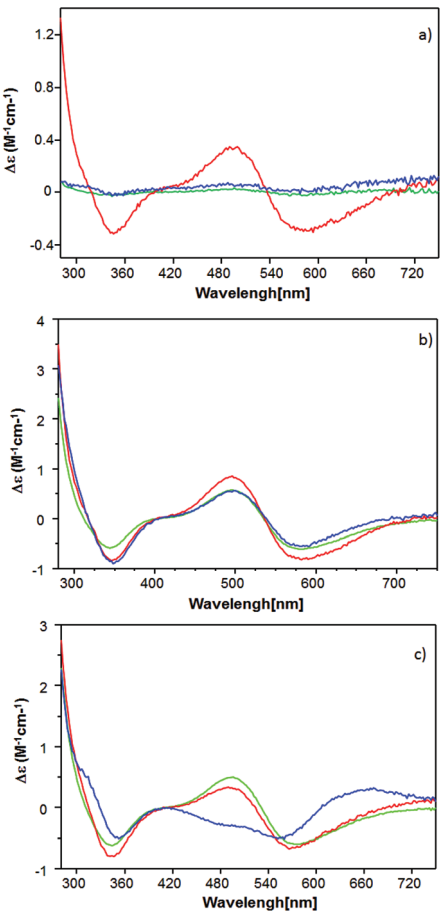

Fig. 2 CD spectra of Cu-AcPVHLDQ-NH_2 (green), Cu-PVHL**N**Q-NH_2 (red), and Cu-**L**VHLDQ-NH_2 (blue) systems at different pH values: (a) pH = 6; (b) pH = 8; (c) pH = 10.5.

The stability constant values are consistent with the involvement of the oxygen atom of the aspartate side chain carboxylate group and the imidazole nitrogen atom, so a 14-membered macrochelate containing a Cu(N_{Im}, O_{Asp}, 2 × O_{water}) chromophore is expected to be formed. CD spectra in the visible region show extremely low intensity features up to pH 6, confirming that Cu(II) binds to donor atoms of quite distant side chains from peptide backbone chiral centres (Fig. 2). UV-Vis parameters support this coordination mode (Table 2).

It is worth noting that $[CuL]^+$ species for both aspartate containing peptides exhibit nearly the same λ_{max} values, hence confirming the participation of the Asp residue side chain in the Cu(II) coordination environment.[27]

Further evidence of carboxylate role in metal complexation is provided indirectly by the analogous complex species $[CuL]^{2+}$ formed by Ac-PVHL**N**Q-NH_2, characterized by a lower stability constant, due to the absence of the oxygen atom of Asp in the Cu(II) coordination environment. The value of $\log\beta$ (3.08) is also lower compared to that of other peptides encompassing only one histidine, thus suggesting the involvement of one imidazole nitrogen atom without any assistance from other atoms,[70,71] as confirmed by the higher λ_{max} value.[27] At pH 6, the CD spectrum show the signal related to the next complex species (Fig. 2a) that begins to form in accordance with the species distribution diagram (Fig. 1b). Indeed, the next species formed by Ac-PVHL**N**Q-NH_2 is $[CuLH_{-1}]^+$; the coordination binding sites for the metal ion may involve imidazole nitrogen and one deprotonated amide nitrogen atom (N_{Im}, N^-) as suggested by the pK value of this deprotonation step. Interestingly, the analogous species is not formed by Ac-PVHLDQ-NH_2 and is formed only in small amounts by Ac-**L**VHLDQ-NH_2, suggesting that macrochelate formation disfavours the first deprotonation step. In fact, the pK value of the deprotonation step for the formation of $[CuLH_{-1}]$ in Ac-**L**VHLDQ-NH_2 is 7.25, more than one unit higher than that observed for the analogous complex formed by Ac-PVHL**N**Q-NH_2.

Table 2 UV-Vis and CD parameters of the Cu(II) complex species formed with Ac-PVHLDQ-NH_2 (**1**), Ac-PVHL**N**Q-NH_2 (**2**) and Ac-LVHLDQ-NH_2 (**3**), respectively

L	Species	UV-Vis λ (nm) (ε (M^{-1} cm^{-1}))	CD λ (nm) ($\Delta\varepsilon$ (M^{-1} cm^{-1}))
1	[CuL]	706 (42)	346 (−0.02), 492 (0.02), 580 (−0.02)
	$[CuLH_{-2}]$	595 (94)	344 (−0.59), 496 (0.57), 582 (−0.61)
	$[CuLH_{-3}]$	540 (98)	334 (−0.65), 474 (0.19), 554 (−0.55)
2	[CuL], $[CuLH_{-1}]^b$	—	345 (−0.31), 491 (0.36), 594 (−0.31)
	$[CuLH_{-2}]$	595 (80)	348 (−0.90), 499 (0.56), 591 (−0.56)
	$[CuLH_{-3}]$	535 ([a])	359 (−0.19), 503 (−1.05), 655 (0.70)
3	[CuL]	705 (45)	345 (−0.03), 491 (0.06), 580 (−0.03)
	$[CuLH_{-2}]$	590 (85)	346 (−0.85), 496 (0.85), 581 (−0.83)
	$[CuLH_{-3}]$	538 (106)	311 (0.739), 346 (−0.28), 496 (−1.60), 628 (0.38)

[a] The formation of a precipitate influenced UV-Vis data. Charges are omitted for clarity. Errors in λ_{max} ± 2 nm, and in ε ± 5%. [b] CD data were recorded at pH 6.

In the pH range 7–9, $[CuLH_{-2}]$ is the predominant species for all these peptides. Owing to metal complex formation, the second amide deprotonation pK value in the Ac-**L**VHLDQ-NH_2 system is lower than the first one. Conversely, the opposite and more usual trend (generally $pK_1 < pK_2$) is observed in the [Cu(Ac-PVHL**N**Q-NH_2)] system (see Table 1). This effect further confirms direct carboxylate involvement in the $[CuL]^+$ species formation as reported above. The consecutive amide deprotonation steps may occur towards the N- or C-termini. In the former case, coordination should occur through the formation of (6,5)-membered chelate rings, generally featuring a higher thermodynamic stability in comparison with the (7,5)-membered chelate rings formed by deprotonation towards the C-terminus.[72–75] Notwithstanding, the involvement of the carboxylic group may favour this last isomer. The UV-Vis parameters suggest a N_3O coordination mode with one imidazole and two amide nitrogen atoms coordinated to the metal ion (N_{Im}, $2 \times N^-$, O_{water}), but the band is broad showing a shoulder at lower wavelength for the proline-containing peptides (Fig. S1†). Taking into account that at pH = 8 the $[CuLH_{-2}]$ species is more than 90% for all copper–peptide systems investigated, the band features suggest the contemporary presence of two isomers.

The CD spectra recorded at pH 8 are similar up to pH 10 for the three copper(II) complex systems (Fig. 2b). There is a wide band around 350 nm and a more intense band in the range 290–310 nm, clearly indicating the involvement of both imidazole and amide nitrogen atoms in the copper coordination sphere. Moreover, the similarity of d–d band transitions suggests that the metal ion experiences a similar chiral environment with the involvement of the same amino acid residues.

The close analogy in the potentiometric and CD data between Ac-PVHLDQ-NH_2 and Ac-**L**VHLDQ-NH_2, considering that residues aspartic/asparagine are more similar than proline/leucine, may suggest that amide deprotonation takes place prevalently towards the C-terminus direction. In this respect, the occurrence of the third amide deprotonation step could provide useful information on the direction in which the process takes place since the peptides Ac-PVHLDQ-NH_2 and Ac-PVHL**N**Q-NH_2 do not have a third amide in the N-terminus.

In fact, both the Ac-PVHLDQ-NH_2 and Ac-PVHL**N**Q-NH_2 peptides form $[CuLH_{-3}]^-$ species on increasing the solution pH, so it becomes the major complex species at pH values higher than 10. The blue-shift of UV-Vis λ_{max}, and the increase in the CD spectra of the $N^- \rightarrow Cu(II)$ charge transfer band at 315 nm, as well as the EPR parameters reported below, clearly indicate the deprotonation of a third amide nitrogen atom that has to occur towards the C-terminus fragment, as the secondary amino acid proline lacks a hydrogen bound to amide.

The pK value of the third deprotonation step for the Cu-Ac-**L**VHLDQ-NH_2 complex is lower in comparison with that of other systems. Indeed, differently from the other two peptides, the third deprotonation steps can also occur towards the N-terminal peptide fragment and potentiometric data indicate a possible increase of the isomer in which deprotonation steps occur towards the N-terminus.[76]

The UV-Vis parameters of $[CuLH_{-3}]$ species are similar to those of the other two peptides, indicating the involvement of four nitrogen atoms in the metal coordination environment, but the differences in the CD spectrum features (Fig. 2c) confirm the presence of two isomers in which the metal ion experiences a different chiral environment. Such an effect is not observed in the analogous species formed with the other two peptides due to the presence of a proline residue in the sequence.

EPR results

EPR data may reveal more detailed information about the metal geometry coordination. $[CuL]^{2+}$ complex species at low pH coexist with the Cu(II) hexa-aqua complex as shown in the corresponding species distribution diagram. Sometimes, EPR studies of frozen solutions can distinguish the features of such Cu(II) complexes from the Cu(II) hexa-aqua ion. However, in this case, any attempts to characterize the [CuL] and $[CuLH_{-1}]$ species by examining low temperature EPR spectra failed, because their parallel resonance features overlap those of the Cu(II) hexa-aqua ion or $[CuLH_{-2}]$, which hinders directly determining their Hamiltonian spin parameters.

On increasing the pH above 7, $[CuLH_{-2}]$ becomes the prevalent species at greater than 80% at physiological pH and it is the sole species present at pH 8. The cooperative deprotonation of two amide nitrogen atoms is clearly corroborated by quite similar magnetic parameters obtained from the EPR spectra of frozen solutions of Cu(II) with the pertinent peptide (Fig. 3 and Table 3).

In fact, a CuN_3O chromophore is in line with such Hamiltonian spin values, although for a square planar Cu(II) environment, slightly lower $g_{\|}$ values and larger absolute $A_{\|}$ values would have been expected. These data could be explained by considering tetrahedral distortion of the square planar geometry, or the formation of a square-based pyramidal geometry. Therefore, an ambiguity in assigning a coordination geometry to these species arises when only spectroscopic UV-Vis EPR parameters are considered. Fortunately, fulfilling this task is greatly helped by their formal square wave voltammetry (SWV) reduction potentials, as well as by DFT calculations (*vide infra*).

The formation of the $[CuLH_{-3}]$ species, with the deprotonation of an additional amide nitrogen atom, becomes significant above pH 10. At this pH value there is a close similarity between the Hamiltonian spin parameters associated with the $[CuLH_{-3}]$ complex species of Ac-PVHLDQ-NH_2 and Ac-PVHL**N**Q-NH_2 ligands. Such Hamiltonian spin parameters imply the formation of a CuN_4 chromophore featuring a tetragonally elongated octahedral coordination environment, with two water molecules occupying the axial positions.

Absolute values of the hyperfine coupling constants for such a chromophore would have been larger than those measured by the experiments. Therefore, even in this case, a significant distortion of the Cu(II) coordination equatorial plane must be expected.

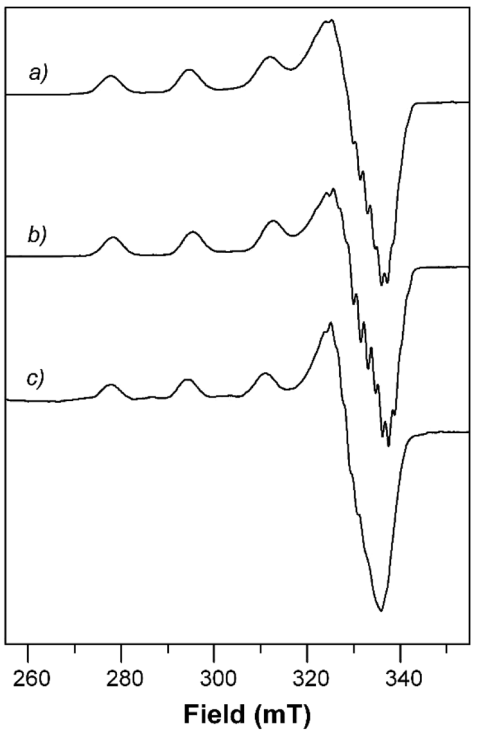

Fig. 3 Frozen-solution EPR spectra at 150 K of 5×10^{-4} M aqueous solution, at pH = 8, of (a) [Cu-(Ac-PVHLDQ-NH_2)H_{-2}]$^-$, (b) [Cu-(Ac-PVHL**N**Q-NH_2)H_{-2}], and (c) [Cu-(Ac-**L**VHLDQ-NH_2)H_{-2}]$^-$ copper complex species.

Table 3 EPR parallel magnetic parameters and formal redox potentials for Cu(II) complex species formed with Ac-PVHLDQ-NH_2 (**1**), Ac-PVHL**N**Q-NH_2 (**2**) and Ac-**L**VHLDQ-NH_2 (**3**), respectively

		EPR		SWV
	Species	$g_\parallel$	$A_\parallel \times 10^4$ cm^{-1}	E_f° (V)/Ag/AgCl
1	[CuL]	—	—	−0.103
	[$CuLH_{-2}$]	2.224	182(546)	−0.125
	[$CuLH_{-3}$]	2.175	194(581)	−0.630
2	[CuL]	—	—	—
	[$CuLH_{-2}$]	2.220	180(540)	−0.140
	[$CuLH_{-3}$]	2.179	196(588)	−0.595
3	[CuL], [$CuLH_{-1}$]	—	—	—
	[$CuLH_{-2}$]	2.230	174(522)	−0.145
	[$CuLH_{-3}$]	2.196	197(591)	−0.550

Errors in $\lambda_{max} \pm 2$ nm, in $\varepsilon \pm 5\%$, in $g_\parallel$ and $A_\parallel \pm 3$ on the last digit and in $E_f \pm 5$ on the last digit; values in parentheses are in MHz.

The different $g_\parallel$ parameters observed for the species formed by the Ac-**L**VHLDQ-NH_2 confirm that the third amide deprotonation may occur prevalently towards the N-terminus shifting the equilibrium towards the (6,5,5) membered chelate rings.

On the whole, potentiometric and spectroscopic data indicate the potential presence of two isomers for the [$CuLH_{-2}$] complexes, for which the carboxyl group may favor coordination toward the C-terminus in the Ac-PVHLDQ-NH_2 peptide. In the Cu-Ac-**L**VHLDQ-NH_2 complex the two isomers may coexist at physiological pH whereas a strong basic pH could favour the third deprotonation step towards the N-terminus.

Voltammetric measurements

EPR results for [$CuLH_{-2}$] species, in particular, Hamiltonian parameters, can be interpreted both as a tetrahedrally distorted square planar geometry and as a square-based pyramidal geometry of the metal coordination environment. To unravel such ambiguities, formal reduction potentials were determined by SWV. In particular, a CuN_3O chromophore with a nearly planar coordination arrangement of the donor atoms is generally characterized by quite a negative formal reduction potential.[77] Conversely, only fairly negative formal reduction potentials were found for all [$CuLH_{-2}$] species, providing convincing evidence of the formation of either a distorted square planar or a square based pyramidal geometry. The formation of tetrahedrally distorted coordination planes can definitively be ruled out, because the formal redox potentials for the [$CuLH_{-2}$] species range from −0.125 to −0.145 V (see Table 3 and Fig. 4), hence a square-based coordination environment can be claimed. Close similarity in formal reduction potentials is observed for the copper(II)–peptide complexes with Ac-PVHL**N**Q-NH_2 and Ac-**L**VHLDQ-NH_2, indicating that the distorted square based pyramidal polyhedra of these systems look

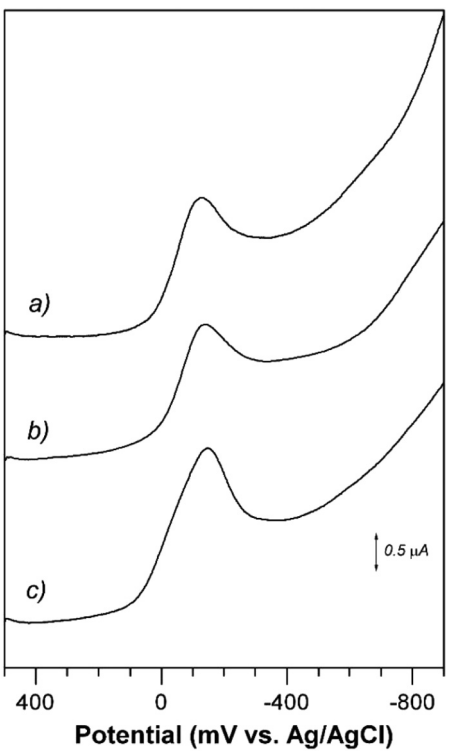

Fig. 4 Square wave voltammograms (30 mV s^{-1}, pulse height 25 mV) of 5×10^{-4} M aqueous solution of (a) [Cu(PVHLDQ)H_{-2}]$^-$, (b) [Cu(PVHL**N**Q)H_{-2}], and (c) [Cu(**L**VHLDQ)H_{-2}]$^-$ copper complex species. All experiments were carried out at pH 8 using 0.1 M KNO_3 as a supporting electrolyte.

alike electrochemically. There seems to be a subtle higher degree of distortion in the [Cu(Ac-PVHLDQ-NH_2)] species, which exhibits a slightly more positive (or less negative) formal reduction potential than the other two analogous complexes.

The formation of [$CuLH_{-3}$] produces electrochemical feedback because the deprotonation of the additional nitrogen amide atom (involved in the coordination to Cu(II)) causes a shift towards much more negative formal reduction potentials. Despite the distortion of the equatorial plane, the formal reduction potentials are still negative enough, with some differences related to the degree of distortion. In particular, the [$CuLH_{-3}$] species of the [Cu(Ac-**L**VHLDQ-NH_2)] system has a less negative formal reduction potential which should correspond to the highest degree of distortion. The distortion of the equatorial plane is also reflected in the $g_{\|}$ value, which is higher than that of the corresponding species with the Ac-PVHL**N**Q-NH_2 peptide. By contrast, the most regular [$CuLH_{-3}$] species corresponds to the [Cu(Ac-PVHLDQ-NH_2)] system which shows the most negative formal reduction potential.

Theoretical calculations of [Cu(Ac-PVHLDQ-NH_2)]$^-$, [Cu(Ac-PVHL**N**Q-NH_2)]^0 and [Cu(Ac-**L**VHLDQ-NH_2)]$^-$ complexes

Coordination modes and molecular geometries. To verify the coordination modes and the molecular geometries, DFT calculations were carried out on the [Cu(Ac-PVHLDQ-NH_2)]$^-$, [Cu(Ac-PVHL**N**Q-NH_2)]^0, and [Cu(Ac-**L**VHLDQ-NH_2)]$^-$ complexes, corresponding to the predominant [$CuLH_{-2}$] species at physiological pH, both *in vacuo* and with 22 water molecules using the protocol described in the Experimental section. As discussed above, potentiometric and spectroscopic results strongly suggest for the [$CuLH_{-2}$] species the coordination of the imidazole and two deprotonated amidic nitrogen atoms. Due to peptide geometry constraints the only coordination mode without relevant geometry distortions of the peptides chain involves the δ-nitrogen of His (N_{His}), the deprotonated amidic nitrogen atoms of Leu and Asp (N_{Leu} and N_{Asp}), and the carboxylic oxygen of Asp (O_{Asp}). Complexes *in vacuo* complete the coordination of the Cu atom by the backbone carbonyl oxygen of Val (O_{Val}), whereas in complexes solvated by the 22 water molecules, coordination can also include one or two water molecules. For the sake of clarity, in the theoretical calculations, the [Cu(Ac-PVHLDQ-NH_2)]$^-$, [Cu(Ac-PVHL**N**Q-NH_2)]^0, and [Cu(Ac-**L**VHLDQ-NH_2)]$^-$ complexes will be generally referred to as **CuL$_A$** (L = hexapeptide), **CuL$_B$** and **CuL$_C$**, respectively. In the [Cu(Ac-PVHL**N**Q-NH_2)]^0 complex, in which Asp is replaced by Asn, the backbone carbonyl oxygen ($O2_{Asn}$) can compete with the carbonyl oxygen of the Asn ($O1_{Asn}$) side chain in coordinating the Cu(II) atom. Therefore, for this complex both coordination modes were investigated, and the labels **CuL$_{B1}$** and **CuL$_{B2}$** will indicate the coordination of $O1_{Asn}$ and $O2_{Asn}$. For the species solvated by the 22 water molecules, the -**W$_{22}$** string is appended to the label of the complex (*e.g.* **CuL$_A$-W$_{22}$**, **CuL$_{B1}$-W$_{22}$**, **CuL$_{B2}$-W$_{22}$** and **CuL$_C$-W$_{22}$**).

It should be noted that the conformational features of the Cu(II)–peptide complexes *in vacuo* are strongly influenced by intramolecular H-bonds, which also give rise to 'artificial' distortions of the peptide chains. By contrast, when the complexes are explicitly solvated with a relatively large number of H_2O molecules, intramolecular interactions are usually lost in favour of the formation of H-bonds with the solvent. Clearly, the calculated energies for the complexes *in vacuo* are affected by both the number of intramolecular H-bonds and the associated steric strain of the chain, so comparing the stabilities of different isomers should be made with caution.

An extensive search on the potential energy surfaces of the three investigated Cu(II)–peptide complexes has led to the characterization of three relevant *in vacuo* isomers. Below, these isomers will be labelled by appending **1**, **2**, and **3** to the complex labels.

In the first set of isomers (**CuL$_X$-1**; **X = A**, **B1**, **B2**, **C**) the Cu(II) atom is penta-coordinated with a distorted trigonal bipyramidal (tbp) geometry with O_{Asp} and N_{Leu} in the apex, and O_{Val}, N_{Asp} and N_{His} in the equatorial positions (see Fig. 5). The three nitrogen atoms are tightly bound to Cu(II), with the Cu–N distances in the range 1.97–2.12 Å (see Fig. 5).

The aspartate carboxylate group in **CuL$_A$-1** and **CuL$_C$-1** also tightly coordinates the metal, the Cu–O_{Asp} distance being slightly smaller than 2 Å. This distance is about 0.1 Å longer in both **CuL$_{B1}$-1** and **CuL$_{B2}$-1**, where the Cu atom is coordinated by an Asn carbonyl oxygen atom. In all complexes the Val (O_{Val}) carbonyl oxygen atom completes the penta-coordination with Cu–O_{Val} distances varying in the range 2.26–2.55 Å.

To quantify the geometrical distortion of the complexes with respect to ideal tbp and square-based pyramidal (sbp) coordination modes, the τ_5 parameter was calculated.[78] This parameter is defined in eqn (3):

$$\tau_5 = \frac{\alpha - \beta}{60^\circ} = 0.01667(\alpha - \beta) \quad (3)$$

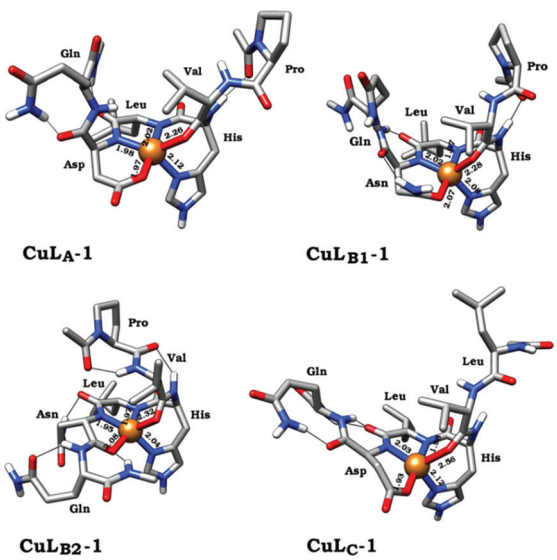

Fig. 5 Schematic representation of the **CuL$_A$-1**, **CuL$_{B1}$-1**, **CuL$_{B2}$-1**, and **CuL$_C$-1** species with selected bond distances (in Å).

α and β being the two largest L–Cu–L bond angles, so that $\tau_5 = 1$ and $\tau_5 = 0$ in complexes with ideal tbp and sbp structures, and distorted complex τ_5 values are between 0 and 1.

The τ_5 values for the **CuL$_A$-1**, **CuL$_{B1}$-1**, **CuL$_{B2}$-1** and **CuL$_C$-1** complexes are 0.58, 0.57, 0.15 and 0.56, respectively, therefore indicating for all these complexes but **CuL$_{B2}$-1** the formation of distorted geometries which can fall between the tbp and the sbp limits. In the case of **CuL$_{B2}$-1**, the low τ_5 value shows that the structure is much better described as sbp rather than tbp.

The second set of isomers (**CuL$_X$-2**; **X** = **A**, **B1**, **B2**, **C**; see Fig. 6) features a geometry similar to the first set, with Cu(II) still penta-coordinated, but approaching a distorted sbp symmetry, in which the imidazole ligand of His moves into the square pyramid plane, and the carbonyl ligand of Val moves to the apex. This apical ligand is not perpendicular to the square plane, but slightly bent toward the His residue. The bond lengths are also similar to those calculated in the first set of isomers: the three nitrogen atoms and O_{Asp} closely coordinate to Cu(II), whereas O_{Val} weakly coordinates the metal ion, with O_{Val}–Cu distances varying between 2.31 and 2.55 Å (Fig. 6). The τ_5 parameters of the **CuL$_A$-2**, **CuL$_{B1}$-2**, **CuL$_{B2}$-2**, and **CuL$_C$-2** complexes are 0.32, 033, 0.16 and 0.13, respectively.

These values show that the structures of **CuL$_A$-2** and **CuL$_{B1}$-2** strongly distort whereas those of **CuL$_{B2}$-2**, and **CuL$_C$-2** are closer to the ideal sbp symmetry. Interestingly, the **CuL$_{B2}$-2** complex value is almost identical to that of **CuL$_{B2}$-1**, indicating that the two isomers feature the same arrangement of ligands, and that differences in the two structures are due only to peptide chain orientations.

In the third set of isomers (**CuL$_X$-3**; **X** = **A**, **B1**, **B2**, **C**), the Val (O_{Val}) carbonyl oxygen atom moves far away from the metal atom, which can therefore be described by a distorted square planar (sp) arrangement of ligands with a CuN_3O coordination mode.

As shown in Fig. 7, the bond distances of the other ligands are not significantly affected by the dissociation of the carbonyl oxygen atom.

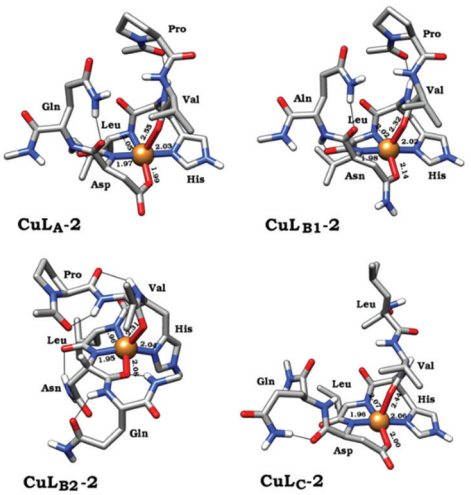

Fig. 6 Schematic representation of the **CuL$_A$-2**, **CuL$_{B1}$-2**, **CuL$_{B2}$-2**, and **CuL$_C$-2** species with selected bond distances (in Å).

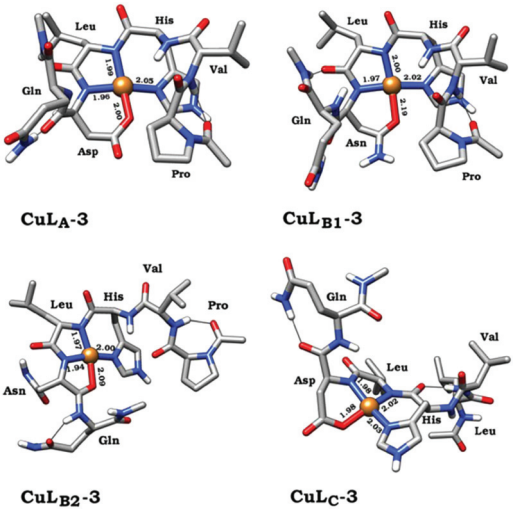

Fig. 7 Schematic representation of the **CuL$_A$-3**, **CuL$_{B1}$-3**, **CuL$_{B2}$-3** and **CuL$_C$-3** species with selected bond distances (in Å).

The relative stabilities of the different isomers are reported in Table S1.† Within the limits discussed above, it can be noted that the square planar configuration is always the most stable, and the square pyramidal arrangement is slightly less stable. On the other hand, the isomers with a trigonal bipyramidal configuration are significantly less stable than the other two isomers. In addition, for the [Cu(Ac-PVHL**N**Q-NH_2)] complex, coordination of the backbone carbonyl oxygen atom of Asn gives the most stable isomer.

Prompted by the above results, solvation with the 22 water molecules was carried out only for the second and third set of isomers. Solvation of the second set of isomers (**X** = **A**, **B1**, **B2**, **C**; see Fig. 8a) did not result in the coordination of a water molecule to the free apex so the coordination mode remained CuN_3O_2. However, the coordination geometries have changed slightly compared to the *in vacuo* complexes.

In particular, in **CuL$_A$-W$_{22}$-2**, the Val (O_{Val}) carbonyl oxygen, which is involved in an H-bond with a water molecule, moves to a much longer distance (2.52 Å) to the *in vacuo* complex. The equatorial Asp carboxylic oxygen also moves to a distance (2.05 Å) further from Cu(II) than in the *in vacuo* complex. The τ_5 value (0.17) is significantly smaller than that calculated for the corresponding *in vacuo* complex, suggesting that the arrangement of ligands approaches the ideal sbp geometry. However, inspection of the complex structure shows that the axial ligand is not perpendicular, but bent with respect to the base of the pyramid toward the His residue, so that the O_{Val}–Cu–N_{Asp} and O_{Val}–Cu–N_{His} angles are 122.4° and 79.7°, a feature that is not captured by the τ_5 parameter.

Structure modifications in the **CuL$_{B1}$-W$_{22}$-2** complex are similar to those discussed for the **CuL$_A$-W$_{22}$-2** complex, but with O_{Val} moving to a still further distance (2.75 Å). Solvation in the **CuL$_{B2}$-W$_{22}$-2** complex has the opposite effect in the coordination of the apical ligand as the Cu–O_{Val} distance decreases from 2.32 Å in the *in vacuo* complex to 2.23 Å in the

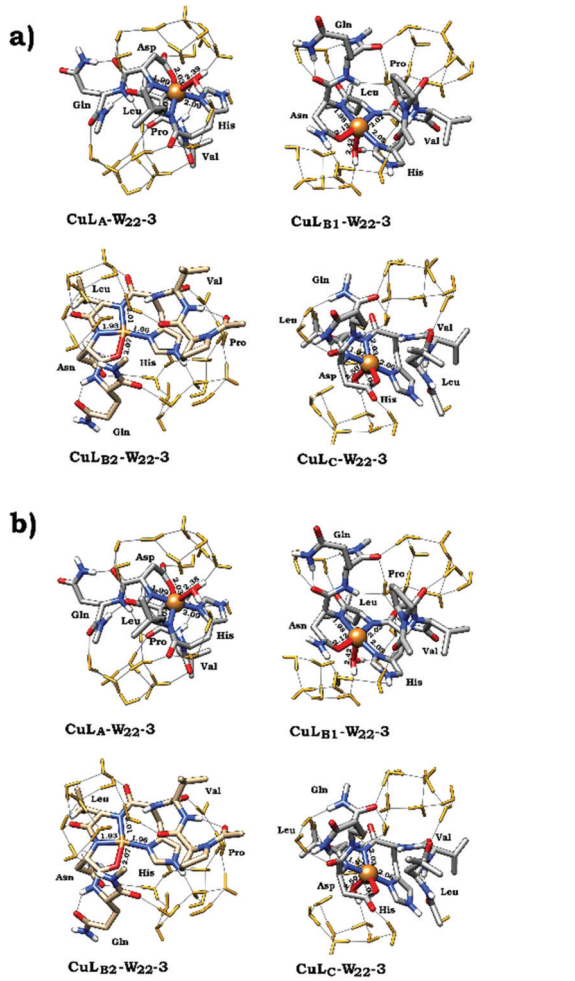

Fig. 8 Schematic representation of (a) **CuL$_X$-W$_{22}$-2** and (b) **CuL$_X$-W$_{22}$-3** species (X = **A**, **B1**, **B2**, **C**) with selected bond distances (in Å).

solvated one. In addition, the apical ligand is almost perpendicular to the base of the pyramid, and therefore the small value of τ_5 (0.04) is really indicative of an almost ideal sbp geometry.

Interestingly, the **CuL$_C$-W$_{22}$-2** complex largely rearranges itself where the O_{Val} leaves the coordination sphere to be replaced at the apex by the backbone carbonyl oxygen of Asp ($O2_{Asp}$). Therefore, in this complex, both $O1_{Asn}$ and $O2_{Asn}$ coordinate the Cu atom simultaneously. In the third set of isomers (**CuL$_X$-W$_{22}$-3**; **X** = **A**, **B1**, **B2**, **C**), solvation with the 22 water molecules leads to coordinating an apical H_2O in all the complexes but **CuL$_{B2}$-W$_{22}$-2**, producing a penta-coordinate species with a distorted square pyramid geometry. In the **CuL$_A$-W$_{22}$-3** complex, the H_2O molecule is at 2.39 Å from the Cu atom, and the N_{Leu}–Cu–O_{Asp} angle is slightly bent (152.5°). A very similar geometry is found for the **CuL$_{B1}$-W$_{22}$-3** complex. Conversely, the **CuL$_{B2}$-W$_{22}$-3** isomer features a square planar tetra-coordination as the apical water molecule is as far as 3.34 Å from Cu(II). Finally, isomer 3 of the $[Cu(Ac\text{-}LVHLDQ\text{-}NH_2)]^-$ complex (**CuL$_C$-W$_{22}$-3**) is still characterized by a weakly coordinated water molecule in the axial position (2.50 Å) and the pyramid plane is slightly distorted with the N_{Leu}–Cu–O_{Asp} angle bent up to the value of 156.3°.

In summary, the most stable ligand configuration of the Cu(II)–peptide complexes exhibits the Cu(II) atom usually penta-coordinated by three nitrogen (N_{Leu}, N_{Asp}, N_{His}) and two oxygen atoms (O_{Asp}, O_{Val}). In the case of CuL$_B$, where Asp is mutated by Asn, the carboxylic oxygen atom (O_{Asp}) is replaced in the coordination by the backbone carbonyl oxygen atom of Asn ($O2_{Asn}$). The coordination geometries in the *in vacuo* complexes are intermediate between a trigonal bipyramid and a square pyramid, whereas the presence of water molecules seems to favour the square pyramidal arrangement. In this case O_{Val} is weakly coordinated axially at distances from Cu(II) which span a large range (2.23–2.84 Å).

EPR hyperfine coupling constants and the *g* values of the isomers of $[Cu(Ac\text{-}PVHLDQ\text{-}NH_2)]^-$, $[Cu(Ac\text{-}PVHLNQ\text{-}NH_2)]^0$ and $[Cu(Ac\text{-}LVHLDQ\text{-}NH_2)]^-$ complexes

Calculated EPR ^{63}Cu hyperfine coupling constants (^{63}Cu-hcc) and *g*-tensors of the species discussed above are collected in Tables 4 and S2,† and compared with the experimental $A_\parallel$ and $g_\parallel$ values. The spin–orbit coupling (relativistic) contributions are important for the Cu(II) ion, due to its relatively large nuclear charge. Therefore, the Fermi contact (FC) and principal values of the dipolar tensor (A_{dip}) are discussed in connection with relativistic corrections (Pseudo Contact (PC), and A_{dip2}). The ^{63}Cu-hcc values are very sensitive to the coordination environment. Generally, the values of $A_\parallel$ increase as geometries change from trigonal bipyramidal to square pyramidal and square planar coordination modes. For the **CuL$_X$-1** (**X** = **A**, **B1**, **B2**, **C**) geometries, which feature a trigonal bipyramidal arrangement of ligands, the ^{63}Cu-hcc exhibit a rhombic symmetry where the $A_\parallel$ component is significantly smaller than the experimental value (see Table 4). **CuL$_{B2}$-1** is an exception which, however, as discussed above, has a geometry approaching the sbp coordination. The ^{63}Cu-hcc of the **CuL$_X$-2** (**X** = **A**, **B1**, **B2**, **C**) complexes, characterized by a distorted square pyramidal geometry, reflect these geometry modifications, as the symmetry of the signal is more axial and the parallel component significantly increases with respect to that calculated for the corresponding first isomers. Notably, in all cases the value of $A_\parallel$ agrees much better with the experiment.

CuL$_X$-3 (**X** = **A**, **B1**, **B2**, **C**) complexes are characterized by a distorted square planar arrangement, with the axial O_{Val} at a very large distance from Cu(II). The $A_\parallel$ component is slightly larger than that calculated for the square pyramidal complexes. It should be noted that the difference in $A_\parallel$ is due to the dipolar component of the tensor as the isotropic component is very similar to that calculated for the other complexes.

Solvation of the **CuL$_A$-2** complex with the water molecules (**CuL$_A$-W$_{22}$-2**) affects the values of ^{63}Cu-hcc compared to the *in vacuo* complex as the $A_\parallel$ component slightly decreases from |−562| to |−534| MHz which agrees very closely with the experiment. In the case of the **CuL$_{B1}$-W$_{22}$-2** complex, the $A_\parallel$ component increases from |−503| MHz for the complex *in vacuo* to |−525| MHz for the solvated complex, probably due

Table 4 ^{63}Cu hyperfine coupling constants (MHz) of the [Cu(Ac-PVHLDQ-NH_2)]$^-$, [Cu(Ac-PVHL**N**Q-NH_2)] and [Cu(Ac-L**V**HLDQ-NH_2)]$^-$ complexes computed using the B3LYP functional and the BS1 basis set on geometries optimized at the RI-BP86/SVP level of theory (for labels see the text)

Complex	A_{FC}[a]	A_{PC}[a]	A_{iso}	A_{dip}[a,b]	A_{dip2}[a,b]	Total dipolar[b]	$A_{\|}$[c]	A_{xx}[c]	A_{yy}[c]	δA_{dip}[d]
CuL_A-1	−273	140	−133	−462, 108, 353	107, −19, −88	−355, 89, 266	−488	−44	133	177
CuL_A-2	−310	117	−192	−470, 252, 218	101, −53, −48	−370, 199, 171	−562	7	−22	29
CuL_A-3	−316	113	−204	−458, 236, 222	95, −44, −51	−363, 186, 273	−567	−18	−26	−8
CuL_A-W_{22}-2	−297	137	−160	−485, 206, 279	111, −48, −63	−374, 158, 215	−534	−2	55	57
CuL_A-W_{22}-3	−288	130	−157	−487, 185, 302	103, −37, −66	−384, 148, 236	−541	−10	79	89
Expt[e]							**546**			
CuL_{B1}-1	−273	134	−140	−443, 61, 382	97, −5, −92	−346, 55, 290	−486	−84	150	234
CuL_{B1}-2	−271	122	−150	−503, −15, 69	101, −32, −69	−353, 135, 219	−503	−15	69	84
CuL_{B1}-3	−300	116	−185	−449, 232, 217	94, −49, −45	−355, 183, 172	−540	−1	−13	12
CuL_{B2}-1	−306	131	−175	−470, 191, 280	107, −44, −63	−363, 147, 217	−538	−28	43	71
CuL_{B2}-2	−304	120	−185	−471, 197, 274	98, −41, −56	−374, 156, 218	−558	−29	33	62
CuL_{B2}-3	−301	109	−202	−459, 236, 224	91, −46, −45	−368, 189, 179	−570	−13	−24	−11
CuL_{B1}-W_{22}-2	−275	124	−151	−476, 227, 249	102, −48, −55	−374, 179, 195	−525	28	44	16
CuL_{B1}-W_{22}-3	−273	135	−138	−486, 225, 261	105, −52, −53	−381, 173, 208	−519	35	70	35
CuL_{B2}-W_{22}-2	−276	120	−156	−488, 230, 258	99, −47, −53	−389, 183, 205	−545	27	49	22
CuL_{B2}-W_{22}-3	−258	118	−140	−479, 226, 253	97, −45, −52	−382, 181, 201	−522	41	62	21
Expt[e]							**540**			
CuL_C-1	−208	122	−86	−451, 100, −208	98, −16, −82	−352, 84, 268	−438	−2	182	184
CuL_C-2	−297	119	−178	−468, 220, 248	100, −48, −52	−369, 173, 196	−547	−6	18	24
CuL_C-3	−307	111	−196	−449, 231, 218	93, −50, −43	−355, 181, 175	−552	−15	−22	−7
CuL_C-W_{22}-2	−231	120	−111	−465, 163, 302	100, −32, −68	−365, 130, 265	−476	19	124	105
CuL_C-W_{22}-3	−281	126	−154	−486, 189, 296	101, −37, −64	−384, 152, 232	−539	−2	78	80
Expt[e]							**522**			

[a] A_{FC} and A_{dip} are non-relativistic Fermi contact and dipolar coupling tensors, respectively. A_{PC} and A_{dip2} are the corresponding relativistic corrections (see ref. 54). [b] The components are reported in the order A_{33}, A_{11}, A_{22}. [c] $A_{\|} = A_{iso} + A_{33}$; $A_{xx} = A_{iso} + A_{11}$; $A_{yy} = A_{iso} + A_{22}$. [d] δA_{dip} is computed as $\delta A_{dip} = A_{22} - A_{11}$ and may be considered as the deviation from the axial symmetry of the tensor. [e] The present work.

to the reduction of the square base distortion. By contrast, the $A_{\|}$ component of the **CuL_{B2}-W_{22}-2** complex decreases compared to the *in vacuo* complex from |−558| to |−545| MHz. It is worth noting that in both cases the $A_{\|}$ component calculated for the solvated complexes agree better with the experimental value of |−540| MHz.

As discussed in the previous section, the **CuL_C-W_{22}-2** complex features a peculiar coordination mode with $O1_{Asp}$ and $O2_{Asp}$ coordinated to Cu(II) at the equatorial and apex positions. Despite the very low τ_5, the ^{63}Cu-hcc has a pronounced rhombic symmetry, with a significantly smaller $A_{\|}$ component than the experimental value.

Solvation of the **CuL_X-3 (X = A, B1, B2, C)** complexes changes the coordination mode as a water molecule weakly coordinates the apex. Therefore, the geometry switches from distorted sp to distorted sbp. For all of the complexes, coordination of the apical water ligand corresponds to a reduction of the ^{63}Cu-hcc tensor $A_{\|}$ component, so the values of the solvated complexes generally agree better with the experiment. Also in the case of the **CuL_{B2}-W_{22}-3** complex, which maintains the square planar coordination (no water molecules coordinated at the apex), we observe a reduction in $A_{\|}$.

The principal components of the complex *g*-tensors are reported in Table S2.† Note that the $g_{\|}$ components are always significantly underestimated with respect to the experimental ones, and are only slightly affected by a specific coordination mode, in agreement with the findings for other Cu(II)–peptide complexes.[74] Therefore, the *g* components are of little help in discriminating different isomeric forms.

For all of the complexes, the unpaired electron is partly delocalized on the atoms coordinating Cu(II), as already observed for other complexes with a similar coordination mode.[79] In particular, atomic spin densities are equal to about 0.55–0.60 on Cu(II) (see Table S3†), and about 0.10–0.15 for the two deprotonated amide nitrogen atoms (N_{Asp}, N_{Leu}). The third nitrogen atom (N_{His}) coordinated to Cu(II) has a lower spin density.

The spin density of the oxygen atom coordinated to the equatorial position is about 0.10 when it belongs to the carboxylic group of the Asp residue, whereas this value decreases to about 0.05 when it belongs to the carbonyl group of the Asn residue. Finally, the oxygen atom weakly coordinating at the apex (O_{val}, O_w) does not feature any spin.

In order to obtain a better insight into the effects of the Cu(II) coordination to the putative binding site on the protein, the [Cu(Ac-PVHLDQ-NH_2)]$^-$ complex in its optimum geometries featuring either O_{Val} or H_2O at the apical position (**CuL_A-W_{22}-2** and **CuL_A-W_{22}-3**, respectively) has been superimposed to the corresponding sequence of the X-ray structure of Ang (see Fig. 9).[80] Superposition has been calculated by minimizing the RMSD of the backbone atoms of the HLD residues directly involved in the Cu binding. It is noteworthy that the backbone atoms of the Cu(II)–peptide complex in the considered region fit reasonably well the X-ray structure of the protein (RMSD =

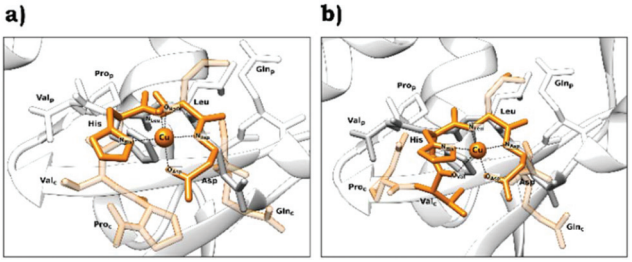

Fig. 9 Superposition of the (a) **CuLA-W_{22}-2** and (b) **CuLA-W_{22}-3** isomers of the [Cu(Ac-PVHLDQ-NH_2)]-complex and the corresponding sequence of the X-ray structure of Ang (X-ray PDB code = 5EOP). Superposition has been calculated by minimizing the RMSD of the backbone atoms of the HLD residues directly involved in the Cu binding. In the figure the [Cu(Ac-PVHLDQ-NH_2)]-complex is drawn in orange and the protein in light grey. The side chains of residues in the [Cu(Ac-PVHLDQ-NH_2)]-complex are labelled with the subscript 'c' whereas the corresponding side chains of the protein are labelled with the subscript 'p'.

1.0 Å), indicating that Cu(II) can bind to this site with only a little structural rearrangement in the protein. This is in agreement with previous experimental UV-Vis CD and NMR results obtained for the whole protein.[33] On the other hand, the side chains of His114 and Asp116 significantly move from their positions in the X-ray structure. In particular, Asp116 should break the H-bond formed with Ser118, providing a local destabilization of the protein structure which may have a functional role in the activity of Ang. Finally, as evident from the superposition of **CuL_A-W_{22}-2** and the protein, the carbonyl oxygen atom of Val cannot coordinate the Cu(II) atom at the apical position, thus allowing exclusion of this coordination mode in the protein.

Conclusions

The angiogenin protein is a potent angiogenic factor in cancers and neurodegenerative diseases. Ang's biological activities are influenced by Cu(II) ions. In many experiments reported in the literature, the protein involved is the recombinant which binds Cu(II) through the terminal amino group of the extra methionine residue. Contrastingly, the protein actually circulating in human plasma has the amino terminus locked in a pyroglutamic ring where His-114 provides the primary coordination site for Cu(II). In metal coordination with the protein, deprotonated amide nitrogen atoms are also present. RNase catalytic activity of Ang is essential for its angiogenic activity, and His-114 is one of the catalytic sites, so the metal binding may drive protein activity.

In this work, combined experimental and computational approaches were employed to characterize the metal binding of the peptide sequence involving the C-terminal sequence of the protein 112–117 (PVHLDQ). Thermodynamic and spectroscopic results highlight that side chain donor atoms of aspartyl and histidyl residues are involved in metal binding at acidic pH and up to 7, and there is evidence that carboxylate is still weakly involved in Cu(II) coordination of the main complex species [$CuLH_{-2}$] formed at physiological pH.

The amide nitrogen deprotonation may occur towards the N- or C-terminus, and two isomers can be formed. Characterization of the Cu(II) complex formed with an analogous peptide in which proline has been substituted by a leucine to mimic a single point mutation present in patients affected by ALS shows similar spectroscopic parameters to those obtained with the Ac-PVHLDQ-NH_2 peptide up to pH 8, whereas some differences in the CD spectra are found at higher pH values. These data suggest that the involvement of the aspartic carboxylic group in Cu(II) coordination may favour the deprotonation towards the C-terminus, while at higher pH the isomers in which deprotonation occurs towards the N-terminus become predominant due to higher thermodynamic stability.

EPR parameters do not discriminate whether the effective copper geometry is either a tetrahedrally distorted square planar or a square based pyramidal geometry. The formal redox potentials for the [$CuLH_{-2}$] species range from −0.125 to −0.145 V, suggesting the latter coordination mode. Theoretical studies were carried out to further confirm this coordination mode and elucidate the specific metal geometry coordination of [$CuLH_{-2}$]. Indeed, the theoretical results are consistent with a CuN_3O_2 coordination mode of Cu(II) with a distorted square pyramidal arrangement of ligands, in which the equatorial positions are occupied by the nitrogen atoms of the deprotonated amides of Asp(Asn) and Leu residues, the δ-N atom of the imidazole of the His residue and the oxygen atom of the carboxylic group of Asp. In the [Cu(Ac-PVHL**N**Q-NH_2)]^0 complex, in which Asp is replaced by Asn, the carboxylic group is replaced by the oxygen atom of the backbone carbonyl group of Asn. This ligand substitution does not significantly affect the values of the hyperfine coupling parameters. The formation of a five membered ring may be the crucial driving force in this replacement. In the other two complexes ([Cu(Ac-PVHLDQ-NH_2)]$^-$ and [Cu(Ac-**L**VHLDQ-NH_2)]$^-$), the preference for a six membered ring is probably due to the much stronger interaction of the charged carboxylic group. Indeed, when starting geometry optimizations from structures featuring the Asp carbonyl oxygen atom coordinated to Cu, this ligand spontaneously dissociated being replaced by an oxygen of the Asp carboxylic group. The apical ligand is an oxygen donor atom weakly coordinated to Cu, and could be either the oxygen atom of the Val carbonyl group or that of a water molecule. The ^{63}Cu-hcc parameters are very similar in both cases, making it difficult to discriminate between the two coordination modes for the complex. We suggest that fluxional behaviour characterizes the complexes with frequent apical ligand interchanges. However, a simple superposition of the complex structures and the corresponding sequence in the X-ray structure of the protein allowed exclusion of the apical coordination of the carbonyl group of Val in the protein. On the other hand, this superposition also shows that the equatorial ligand can bind the copper atom without significant rearrangement of the protein structure.

Acknowledgements

A. Magrì, G. Tabbì, R. P. Bonomo and D. La Mendola acknowledge the University Consortium for Research in the Chemistry of the Metal Ions in Biological Systems (CIRCMSB).

Notes and references

1 D. J. Strydom, J. W. Fett, R. R. Lobb, E. M. Alderman, J. L. Bethune, J. F. Riordan and B. L. Vallee, *Biochemistry*, 1985, **24**, 5486–5494.
2 B. L. Vallee and J. F. Riordan, *Cell. Mol. Life Sci.*, 1997, **53**, 803–815.
3 A. Tello-Montoliu, J. V. Patel and G. Y. H. Lip, *J. Thromb. Haemostasis*, 2006, **4**, 1864–1874.
4 K. Kishimoto, S. Liu, T. Tsuji, K. A. Olson and G.-F. Hu, *Oncogene*, 2005, **24**, 445–456.
5 N. Yoshioka, L. Wang, K. Kishimoto, T. Tsuji and G. Hu, *Proc. Natl. Acad. Sci. U. S. A.*, 2006, **103**, 14519–14524.
6 C. Bárcena, M. Stefanovic, A. Tutusaus, G. A. Martinez-Nieto, L. Martinez, C. García-Ruiz, A. de Mingo, J. Caballeria, J. C. Fernandez-Checa, M. Marí and A. Morales, *Sci. Rep.*, 2015, **5**, 7916.
7 J. W. Fett, D. J. Strydom, R. R. Lobb, E. M. Alderman, J. L. Bethune, J. F. Riordan and B. L. Vallee, *Biochemistry*, 1985, **24**, 5480–5486.
8 J. Folkman and P. A. D'amore, *Cell*, 1996, **87**, 1153–1155.
9 D. J. Strydom, *Cell. Mol. Life Sci.*, 1998, **54**, 811–824.
10 M. Moenner, M. Gusse, E. Hatzi and J. Badet, *Eur. J. Biochem.*, 1994, **226**, 483–490.
11 S. Li and G.-F. Hu, *J. Cell. Physiol.*, 2012, **227**, 2822–2826.
12 V. Subramanian and Y. Feng, *Hum. Mol. Genet.*, 2007, **16**, 1445–1453.
13 S. Li and G. F. Hu, *Int. J. Biochem. Mol. Biol.*, 2010, **1**, 26–35.
14 T. U. Steidinger, S. R. Slone, H. Ding, D. G. Standaert and T. A. Yacoubian, *PLoS One*, 2013, **8**, e56092.
15 Y. N. Kim and D. H. Kim, *Prog. Neuro-Psychopharmacol. Biol. Psychiatry*, 2012, **38**, 116–120.
16 W. Qin, X. Jia, F. Wang, X. Zuo, L. Wu, A. Zhou, D. Li, B. Min, C. Wei, Y. Tang, Y. Xing, X. Dong, Q. Wang, Y. Gao, Y. Li and J. Jia, *J. Alzheimer's Dis.*, 2015, **45**, 245–252.
17 M. J. Greenway, P. M. Andersen, C. Russ, S. Ennis, S. Cashman, C. Donaghy, V. Patterson, R. Swingler, D. Kieran, J. Prehn, K. E. Morrison, A. Green, K. R. Acharya, R. H. Brown and O. Hardiman, *Nat. Genet.*, 2006, **38**, 411–413.
18 H. Kishikawa, D. Wu and G. Hu, *Expert Opin. Ther. Targets*, 2008, **12**, 1229–1242.
19 D. Wu, W. Yu, H. Kishikawa, R. D. Folkerth, A. J. Iafrate, Y. Shen, W. Xin, K. Sims and G. F. Hu, *Ann. Neurol.*, 2007, **62**, 609–617.
20 J. H. Kaplan and S. Lutsenko, *J. Biol. Chem.*, 2009, **284**, 25461–25465.
21 C. M. Opazo, M. A. Greenough and A. I. Bush, *Front. Aging Neurosci.*, 2014, 6.
22 S. A. Lowndes and A. L. Harris, *J. Mammary Gland Biol. Neoplasia*, 2005, **10**, 299–310.
23 G. J. Brewer, *J. Trace Elem. Med. Biol.*, 2014, **28**, 372–378.
24 L. Finney, S. Mandava, L. Ursos, W. Zhang, D. Rodi, S. Vogt, D. Legnini, J. Maser, F. Ikpatt, O. I. Olopade and D. Glesne, *Proc. Natl. Acad. Sci. U. S. A.*, 2007, **104**, 2247–2252.
25 J. Badet, F. Soncin, J. D. Guitton, O. Lamare, T. Cartwright and D. Barritault, *Proc. Natl. Acad. Sci. U. S. A.*, 1989, **86**, 8427–8431.
26 F. Soncin, J. D. Guitton, T. Cartwright and J. Badet, *Biochem. Biophys. Res. Commun.*, 1997, **236**, 604–610.
27 D. La Mendola, A. Magrì, L. I. Vagliasindi, Ö. Hansson, R. P. Bonomo and E. Rizzarelli, *Dalton Trans.*, 2010, **39**, 10678–10684.
28 L. Bertini, M. Bruschi, M. Romaniello, G. Zampella, M. Tiberti, V. Barbieri, C. Greco, D. La Mendola, R. P. Bonomo, P. Fantucci and L. De Gioia, *Theor. Chem. Acc.*, 2012, **131**, 1–15.
29 D. La Mendola, D. Farkas, F. Bellia, A. Magrì, A. Travaglia, O. Hansson and E. Rizzarelli, *Inorg. Chem.*, 2012, **51**, 128–141.
30 A. Magrì, A. Munzone, M. Peana, S. Medici, M. A. Zoroddu, O. Hansson, C. Satriano, E. Rizzarelli and D. La Mendola, *Int. J. Mol. Sci.*, 2016, **17**, E1240.
31 G. F. Hu, *J. Cell. Biochem.*, 1998, **69**, 326–335.
32 E. Shapiro, R. Wade Harper, J. Fox, E. A. Jansen, H. W. Friedrich and H. Uhlmann, *Anal. Biochem.*, 1988, **175**, 450–461.
33 D. La Mendola, F. Arnesano, Ö. Hansson, C. Giacomelli, V. Calò, V. Mangini, A. Magrì, F. Bellia, M. L. Trincavelli, C. Martini, G. Natile and E. Rizzarelli, *Metallomics*, 2016, **8**, 118–124.
34 C. Giacomelli, M. L. Trincavelli, C. Satriano, Ö. Hansson, D. La Mendola, E. Rizzarelli and C. Martini, *Int. J. Biochem. Cell Biol.*, 2015, **60**, 185–196.
35 J. Moroianu and J. F. Riordan, *Proc. Natl. Acad. Sci. U. S. A.*, 1994, **91**, 1677–1681.
36 A. Pal, M. Siotto, R. Prasad and R. Squitti, *J. Alzheimer's Dis.*, 2015, **44**, 343–354.
37 J. T. Rubino and K. J. Franz, *J. Inorg. Biochem.*, 2012, **107**, 129–143.
38 L. D. Pettit and R. A. Robbins, in *Handbook of Metal Ligand Interaction in Biological Fluids*, ed. G. Berthon, Marcel Dekker, New York, 1995, vol. 1, pp. 636–656.
39 M. Łuczkowski, H. Kozlowski, M. Stawikowski, K. Rolka, E. Gaggelli, D. Valensin and G. Valensin, *J. Chem. Soc., Dalton Trans.*, 2002, 2269–2274.
40 G. Arena, D. La Mendola, G. Pappalardo, I. Sóvágó and E. Rizzarelli, *Coord. Chem. Rev.*, 2012, **256**, 2202–2218.
41 D. La Mendola, R. P. Bonomo, G. Impellizzeri, G. Maccarrone, G. Pappalardo, A. Pietropaolo, E. Rizzarelli and V. Zito, *J. Biol. Inorg. Chem.*, 2005, **10**, 463–475.
42 P. Gans, A. Sabatini and A. Vacca, *Talanta*, 1996, **43**, 1739–1753.

43 L. Alderighi, P. Gans, A. Ienco, D. Peters, A. Sabatini and A. Vacca, *Coord. Chem. Rev.*, 1999, **184**, 311–318.
44 A. D. Becke, *Phys. Rev. A*, 1988, **38**, 3098–3100.
45 J. P. Perdew, *Phys. Rev. B: Condens. Matter*, 1986, **33**, 8822–8824.
46 K. Eichkorn, O. Treutler, H. Ohm, M. Haser and R. Ahlrichs, *Chem. Phys. Lett.*, 1995, **240**, 283–289.
47 A. Schäfer, H. Horn and R. Ahlrichs, *J. Chem. Phys.*, 1992, **97**, 2571–2577.
48 M. Elstner, D. Porezag, G. Jungnickel, J. Elsner, M. Haugk, T. Frauenheim, S. Suhai and G. Seifert, *Phys. Rev. B: Condens. Matter*, 1998, **58**, 7260–7268.
49 T. Frauenheim, G. Seifert, M. Elstner, Z. Hajnal, G. Jungnickel, D. Porezag, S. Suhai and R. Scholz, *Phys. Status Solidi*, 2000, **217**, 41–62.
50 C. Kohler, G. Seifert, U. Gerstmann, M. Elstner, H. Overhof and T. Frauenheim, *Phys. Chem. Chem. Phys*, 2001, **3**, 5109–5114.
51 T. Kruger, M. Elstner, P. Schiffels and T. Frauenheim, *J. Phys. Chem.*, 2005, **122**, 114110–114115.
52 B. Aradi, B. Hourahine and T. Frauenheim, *J. Phys. Chem. A*, 2007, **111**, 5678–5684.
53 M. Elstner, *J. Phys. Chem. A*, 2007, **111**, 5614–5621.
54 M. Bruschi, L. Bertini, V. Bonačić-Koutecký, L. De Gioia, R. Mitrić, G. Zampella and P. Fantucci, *J. Phys. Chem. B*, 2012, **116**, 6250–6260.
55 A. D. Becke, *J. Chem. Phys.*, 1993, **98**, 5648–5652.
56 S. H. Vosko, L. Wilk and M. Nusair, *Can. J. Phys.*, 1980, **58**, 1200–1211.
57 C. Lee, W. Yang and R. Parr, *Phys Rev B: Condens. Matter*, 1988, **37**, 785–789.
58 P. J. Stephens, F. J. Devlin, C. F. Chabalowski and M. J. Frisch, *J. Phys. Chem.*, 1994, **98**, 11623–11627.
59 W. Kutzelnigg, U. Fleischer and M. Schindler, in *Deuterium, Shift Calculation*, 1991, vol. 23, pp. 165–262.
60 B. A. Heß, C. M. Marian, U. Wahlgren and O. Gropen, *Chem. Phys. Lett.*, 1996, **251**, 365–371.
61 M. Kaupp, M. Bühl and V. G. Malkin, *Calculation of NMR, EPR parameters. Theory, Applications*, Wiley VCH, 2004, pp. 3–527.
62 R. Ahlrichs, M. Bär, M. Häser, H. Horn and C. Kölmel, *Chem. Phys. Lett.*, 1989, **162**, 165–169.
63 F. Neese, *Wiley Interdiscip. Rev.: Comput. Mol. Sci.*, 2012, **2**, 73–78.
64 C. Kállay, K. Várnagy, G. Micera, D. Sanna and I. Sóvágó, *J. Inorg. Biochem.*, 2005, **99**, 1514–1525.
65 B. Bóka, A. Myari, I. Sóvágó and N. Hadjiliadis, *J. Inorg. Biochem.*, 2004, **98**, 113–122.
66 D. La Mendola, A. Magrì, Ö. Hansson, R. P. Bonomo and E. Rizzarelli, *J. Inorg. Biochem.*, 2009, **103**, 758–765.
67 C. Kállay, Z. Nagy, K. Várnagy, G. Malandrinos, N. Hadjiliadis and I. Sóvágó, *Bioinorg. Chem. Appl.*, 2007, 30394.
68 I. Sóvágó and K. Osz, *Dalton Trans.*, 2006, 3841–3854.
69 D. La Mendola, A. Magrì, T. Campagna, M. A. Campitiello, L. Raiola, C. Isernia, O. Hansson, R. P. Bonomo and E. Rizzarelli, *Chem. – Eur. J.*, 2010, **16**, 6212–6223.
70 H. Kozłowski, W. Bal, M. Dyba and T. Kowalik-Jankowska, *Coord. Chem. Rev.*, 1999, **184**, 319–346.
71 A. Magrì, F. D'Alessandro, D. A. Distefano, T. Campagna, G. Pappalardo, G. Impellizzeri and D. La Mendola, *J. Inorg. Biochem.*, 2012, **113**, 15–24.
72 J. F. Galey, B. Decock-Le Reverend, A. Lebkiri, L. D. Pettit, S. I. Pyburn and H. Kozlowski, *J. Chem. Soc., Dalton Trans.*, 1991, 2281–2287.
73 R. R. Khoury, G. J. Sutton, D. Ebrahimi and D. B. Hibbert, *Inorg. Chem.*, 2014, **53**, 1278–1287.
74 A. Kadej, M. Kuczer and T. Kowalik-Jankowska, *Dalton Trans.*, 2015, **44**, 20659–20674.
75 A. Magrì, D. La Mendola, V. G. Nicoletti, G. Pappalardo and E. Rizzarelli, *Chem. – Eur. J.*, 2016, **22**, 13287–13300.
76 T. Kowalik-Jankowska, E. Jankowska, Z. Szewczuk and F. Kasprzykowski, *J. Inorg. Biochem.*, 2010, **104**, 831–842.
77 G. Tabbì, A. Giuffrida and R. P. Bonomo, *J. Inorg. Biochem.*, 2013, **128**, 137–145.
78 A. W. Addison, T. N. Rao, J. Reedijk, J. van Rijn and G. C. Verschoor, *J. Chem. Soc., Dalton Trans.*, 1984, **9**, 1349–1356.
79 M. Bruschi, L. De Gioia, R. Mitrić, V. Bonacić-Koutecký and P. Fantucci, *Phys. Chem. Chem. Phys.*, 2008, **10**, 4573–4583.
80 D. S. M. Chatzileontiadou, V. G. Tsirkone, K. Dossi, A. G. Kassouni, P. V. G. Liggri, A. L. Kantsadi, G. A. Stravodimos, N. A. Balatsos, V. T. Skamnaki and D. D. Leonidas, *FEBS Lett.*, 2016, **590**, 3005–3018.